RESEARCH ARTICLE
ATMOSPHERIC PHYSICS

Earth and Planetary Physics
9: 54–68, 2025
doi: 10.26464/epp2024030

Mesospheric tide comparisons at low latitudes observed by two collocated meteor radars

Jian Li[1,2], Wen Yi[1,2*], XiangHui Xue[1,2,3,4*], Jie Zeng[1,2], HaiLun Ye[1,2], JianYuan Wang[1,5,6], JinSong Chen[5,6], Na Li[5,6], and TingDi Chen[1,2]

[1]Chinese Academy of Sciences (CAS) Key Laboratory of Geospace Environment, Department of Geophysics and Planetary Sciences, University of Science and Technology of China, Hefei 230026, China;

[2]CAS Center for Excellence in Comparative Planetology, Anhui Mengcheng Geophysics National Observation and Research Station, University of Science and Technology of China, Hefei 230026, China;

[3]Hefei National Laboratory, University of Science and Technology of China, Hefei 230026, China;

[4]Collaborative Innovation Center of Astronautical Science and Technology, Harbin 150001, China;

[5]National Key Laboratory of Electromagnetic Environment, China Research Institute of Radiowave Propagation, Qingdao 266107, China;

[6]Yunnan Kunming Electromagnetic Environment National Observation and Research Station, Qujing Kunming 655000, China

Key Points:

- A comparison of mesospheric tides observed by two collocated meteor radars is presented.
- Seasonal variations of the diurnal, semidiurnal, and terdiurnal tides at low latitudes are reported.
- The statistical analysis approach provides an estimation of the uncertainties associated with mesospheric tides observed by the meteor radar.

Citation: Li, J., Yi, W., Xue, X. H., Zeng, J., Ye, H. L., Wang, J. Y., Chen, J. S., Li, N., and Chen, T. D. (2025). Mesospheric tide comparisons at low latitudes observed by two collocated meteor radars. *Earth Planet. Phys.*, *9*(1), 54–68. http://doi.org/10.26464/epp2024030

Abstract: Accurate knowledge of mesospheric winds and waves is essential for studying the dynamics and climate in the mesosphere and lower thermosphere (MLT) region. In this study, we conduct a comparative analysis of the mesosphere tidal results obtained from two adjacent meteor radars at low latitudes in Kunming, China, from November 2013 to December 2014. These two radars operate at different frequencies of 37.5 MHz and 53.1 MHz, respectively. However, overall good agreement is observed between the two radars in terms of horizontal winds and tide observations. The results show that the dominant tidal waves of the zonal and meridional winds are diurnal and semidiurnal tides. Moreover, we conduct an exhaustive statistical analysis to compare the tidal amplitudes and vertical wavelengths recorded by the dual radar systems, which reveals a high degree of alignment in tidal dynamics. The investigation includes variances and covariances of tidal amplitudes, which demonstrate remarkable consistency across measurements from both radars. This finding highlights clear uniformity in the mesospheric tidal patterns observed at low latitudes by the two neighboring meteor radars. Results of the comparative analysis specifically underscore the significant correlation in vertical wavelength measurements, validating the robustness of radar observations for tidal research.

Keywords: mesosphere and lower thermosphere region; meteor radar; mesospheric winds; tides

1. Introduction

The mesosphere and lower thermosphere (MLT) region is a crucial transitional region in Earth's atmosphere, located at altitudes between approximately 60 and 120 km. This region serves as a significant connection area through which numerous atmospheric waves propagate, including planetary waves (Forbes, 1995; Espy et al., 2005; Wang JC et al., 2021; He MS, 2023), tides (Forbes and Garrett, 1979), and gravity waves (Allen and Vincent, 1995; Fritts and Alexander, 2003), coupling the lower and upper atmosphere (Vincent, 2015). Consequently, the observation of these atmospheric waves through ground-based instruments or satellites is of paramount importance for gaining insights into the dynamic atmospheric processes within this region and, in turn, for studying the coupling between different atmospheric layers. Among them, atmospheric tides are significant waves that can dominate the dynamics in the MLT region.

Atmospheric tides are global-scale atmospheric waves with periods that are harmonics of the solar day (Chapman and Lindzen, 1970; Hagan, 1996; Baumgarten and Stober, 2019). Tides are primarily generated in the troposphere and stratosphere, and

First author: J. Li, lj01511@mail.ustc.edu.cn
Correspondence to: W. Yi, yiwen@ustc.edu.cn
X. H. Xue, xuexh@ustc.edu.cn
Received 13 DEC 2023; Accepted 05 APR 2024.
First Published online 05 JUN 2024.

then propagate vertically to the MLT region, where they reach significant amplitudes. These atmospheric tides can be categorized as migrating and nonmigrating tides. Migrating tides propagate westward with the apparent motion of the sun, whereas nonmigrating tides can propagate eastward, westward, or remain stationary (Forbes, 1984; Vial, 1989; Vitharana et al., 2021). Migrating diurnal and semidiurnal tides are the predominant modes that have been extensively studied (Gong Y et al., 2013; Yu Y et al., 2013; Xiong C et al., 2015; Wang JY et al., 2022, and the references therein). Their strong vertical upward propagation of energy and momentum from the lower atmosphere significantly affects the dynamics of the mesosphere (Forbes and Garrett, 1979; Forbes, 1995).

In recent decades, meteor radars (MRs) have found widespread application in the study of the MLT region. Meteor radars offer advantages such as cost-effectiveness, ease of installation, and the ability to operate continuously under all weather conditions, making them the most widely used conventional instruments for MLT wind observations (Hocking et al., 2001; Holdsworth et al., 2004). Meteor radars operate around the clock, regardless of day or night, and they function effectively under geographical conditions, allowing for robust long-term observations. Consequently, MRs have proven to be a potent technology for researching the dynamics and sclimate of the middle atmospheric region, including aspects such as wind fields (Yi W et al., 2019; Gu SY et al., 2021; Stober et al., 2021; Zhou BZ et al., 2022; Long C et al., 2023), neutral density (Takahashi et al., 2002; Stober et al., 2014), temperature (Hocking, 1999; Hall et al., 2012), planetary waves (Kishore et al., 2018; He MS and Forbes, 2022), and tidal waves (Jacobi et al., 2017; He MS and Chau, 2019; Spargo et al., 2019; Liu GP et al., 2022).

To gain a better understanding of the actual atmospheric tidal waves, it is meaningful to compare observations from different instruments or the same instrument. Several comparisons have been conducted to date. Cervera and Reid (1995) conducted a comparison of the semidiurnal tidal amplitudes and phases at the same location by using a very high frequency (VHF) MR operating at 54.1 MHz and a medium frequency (MF) radar operating at 1.98 MHz. The authors concluded that the semidiurnal tidal phases and amplitudes below 92 km were highly consistent between the two technologies at all altitudes. Above 92 km, the MR exhibited larger tidal amplitudes. Hocking and Thayaparan (1997) showed good agreement in their observations of diurnal and semidiurnal tides between the MF radar and MR in London, Canada (43°N, 81°W). In addition, comparing the same instruments at different locations is meaningful for studying the tidal spatial (altitude and latitude) structure. Pancheva et al. (2021) conducted a study on terdiurnal (8-h) and quarterly diurnal (6-h) tides by using two MRs located in Tromsø (70°N, 19°E) and Svalbard (78°N, 16°E), Norway. They not only observed distinct seasonal variations but also identified structural differences in altitude between the two tides. They explained that the dominant tidal mode or modes have an appreciable structure in the latitudinal direction (i.e., they are represented by Hough modes with multiple maxima and minima). The results of their research have contributed significantly to enhancing our understanding of the forcing mechanisms responsible for these short-period tides at high latitudes.

In this study, we utilize measurements of neutral winds in the MLT region obtained from two collocated MRs located at Kunming, China (25.6°N, 103.8°E). We then conduct an intercomparison of mesospheric tides based on these measurements. Moreover, we use statistical methods to quantitatively assess their consistency. The structure of the remaining sections of this article is as follows: In Section 2, we introduce the MRs and the associated dataset. Then, in Section 3, we report on our comparative analysis of the seasonal variations in mesospheric winds and tides observed by the two collocated MRs. In Section 4, we describe the statistical comparison of tides observed by these two collocated MRs. Finally, we summarize our results.

2. Data and Method

2.1 Kunming Meteor Radars

The Kunming meteor radars (KMMRs) are installed at the Kunming Electromagnetic Environment Observation and Research Station (25.6°N, 103.8°E) in Yunnan Province, China. The KMMRs are operated by the China Research Institute of Radiowave Propagation (Yi W et al., 2014, 2018). One of the two MRs is a dedicated 37.5 MHz "all-sky" interferometric MR, closely mirroring the system detailed by Holdsworth et al. (2004), whereas the other is a 53.1 MHz stratospheric–tropospheric MR (ST/MR), exhibiting similarities to the configuration outlined by Reid et al. (2006). The separation between the two MR antenna arrays is approximately 300 m, and we provide a summary of the operational parameters for both KMMRs in Table 1. Note that the two MRs are different only in regard to their operating frequency and peak power.

Meteor counts and neutral wind fields have been investigated by Zeng J et al. (2022) using these two KMMRs. Their findings provide a critical context for our work, particularly in validating our extraction techniques and understanding the mesospheric wind patterns that influence tidal dynamics. Building on this work, in the present study, we utilize data obtained by the two KMMRs from November 1, 2013, to December 31, 2014, including hourly measurements of horizontal zonal and meridional winds with a

Table 1. Main operating parameters of the two Kunming meteor radars.

Parameter	37.5 MHz radar	53.1 MHz radar
Pulse repetition frequency	430 Hz	430 Hz
Peak power	20 kW	40 kW
Range resolution	1.8 km	1.8 km
Pulse type	Gaussian	Gaussian
Pulse width	24 μs	24 μs

2-km height resolution. This dataset is used to investigate the seasonal variations in horizontal wind and to extract mesospheric tides in the MLT regions at northern low latitudes.

2.2 Method

The amplitudes and phases of diurnal, semidiurnal, and terdiurnal tides are determined by applying the least squares fitting method to the hourly wind data of zonal and meridional winds. In this study, a 7-d data window, sliding forward by 1 d, is utilized for tide extraction. Subsequently, the average over the 7 d, including 3 d before and 3 days after each time point, is calculated to obtain a 24-h composite wind. Each component of the wind can be expressed as

$$y(t) = \bar{y}(t) + \sum_{i=1}^{3} A_i \sin\left(\frac{2\pi i}{24}t + \phi_i\right), \tag{1}$$

where $y(t)$ is wind measurements, $\bar{y}(t)$ is the prevailing component, and A_i and ϕ_i represent the amplitude and phase, respectively (Wu DL et al., 1995). In this article, for convenience, we have translated the phase from radians into local time notation. The tidal components with periods of 24, 12, and 8 h represent the diurnal, semidiurnal, and terdiurnal tides, respectively (Baumgarten and Stober, 2019; Yi W et al., 2023).

This methodology enables the precise extraction of tidal signal amplitudes and phases, facilitating subsequent comparisons and analyses. It offers a comprehensive understanding of the relationships and consistencies between the tidal components observed by the two KMMRs.

3. Seasonal Variations in MLT Winds and Tides Observed by the Two KMMRs

Figure 1 shows the monthly mean zonal and meridional wind between altitudes of 76 and 100 km from November 2013 to December 2014. Data gaps are present around 100 km because of a lack of meteor observations, leading to missing wind speed inversion data. Nevertheless, the available information offers good continuity for studying atmospheric dynamics and climatology in the MLT region at low latitudes. The seasonal variations in zonal and meridional winds observed by the two KMMRs show remarkably consistent patterns throughout the seasons. Below 84 km, both zonal wind components exhibit an annual variation. In winter (December), a strong eastward wind occurs with a maximum of approximately 40 m/s, whereas in spring (March to May), a weak westward wind is observed with a maximum of approximately 20 m/s. Above 84 km, both zonal wind components show an annual variation. A strong eastward wind occurs during summer (June to August), with a maximum of approximately 30 m/s, and a weak westward wind occurs during winter (December), with a maximum of approximately 5 m/s.

Figures 1c and 1d show the monthly mean variation in meridional wind. Both meridional wind components mainly show annual variation with a strong northward wind during winter, with a maximum of approximately 30 m/s below 90 km, and a southward wind during spring (February to April) with a maximum of approximately 25 m/s above 90 km. Gong Y et al. (2020) showed a similar structure in the neutral wind at Wuhan station (30.5°N, 114.6°E). The two MR observations show slight local differences. Above 94 km, the meridional wind speed observed by the 37.5 MHz meteor radar is higher than that observed by the 53.1 MHz meteor radar. This difference may be attributed to the lower meteor count above this altitude, leading to a larger error in wind speed retrieval. In general, the wind field comparisons between the two radars show strong consistency and are the same as the results of Zeng J et al. (2022). This initial observation suggests the feasibility and reliability of the tidal comparisons in the data.

Moreover, we estimate the atmospheric tide by using the hourly wind. We investigate the seasonal variation in the solar tides in the MLT wind observed by the two KMMRs.

The Lomb–Scargle method is a powerful tool for showing the

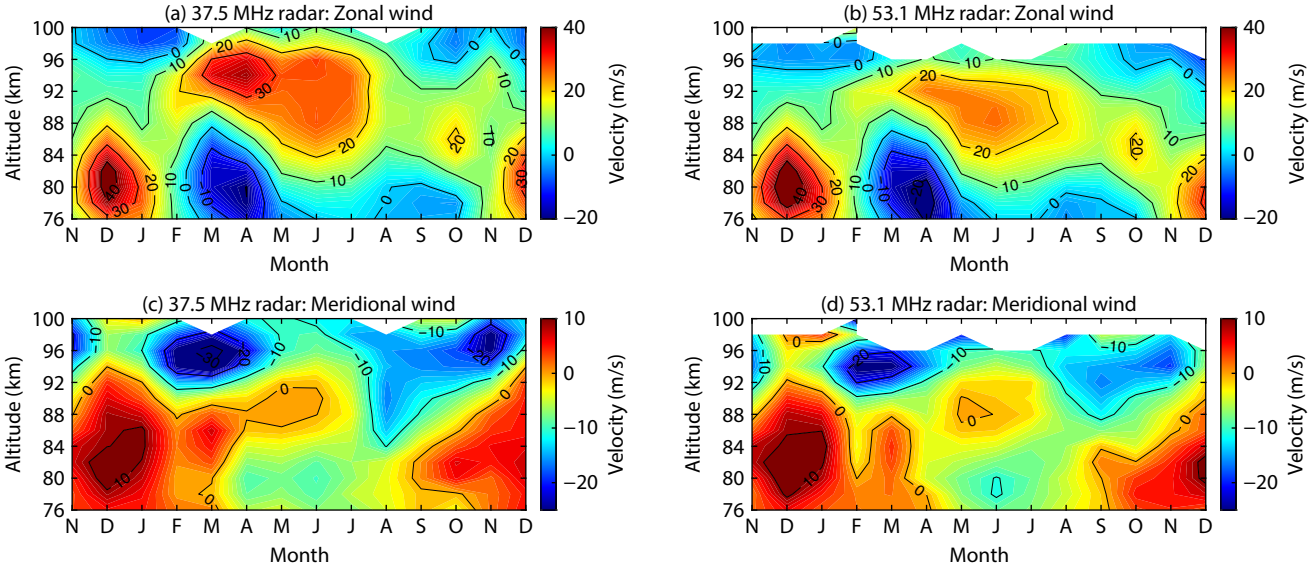

Figure 1. (a) 37.5 MHz MR and (b) 53.1 MHz MR monthly mean zonal winds (eastward is positive) and (c) 37.5 MHz MR and (d) 53.1 MHz MR meridional winds (northward is positive) from November 2013 to December 2014 observed by the KMMRs between altitudes of 76 and 100 km.

dominant oscillation modes in a time series with gaps (Lomb, 1976; Scargle, 1982). Figure 2 shows the Lomb–Scargle periodogram of zonal and meridional hourly winds at an altitude of 90 km. It is clear that the dominant tidal wave of the zonal and meridional winds observed by the two KMMRs are diurnal and semidiurnal tides.

The periodograms of 8 h and 6 h corresponding to the terdiurnal and quarterly diurnal tides can also be observed by the two KMMRs. However, these amplitudes are much weaker than those of the diurnal and semidiurnal tides, which is in line with the results found by Guharay et al. (2013) based on meteor radar observations in Brazil at São João do Cariri (7.41°S, 36.51°W). Additionally, periods near 2 d and 5 d are observed, which are likely indicative of planetary wave activity (e.g., Gu SY et al., 2017).

To directly compare the tidal dynamics derived from the MLT wind observations by the two KMMRs, we composite the hourly variation in mean zonal and meridional winds divided into four seasons. In Figure 3, we also show examples of tidal structures during the spring and autumn equinoxes and the summer and winter solstices from November 2013 to December 2014. In general, the hourly wind observations from both radars exhibit strong similarities, and the vertical tidal structures in both cases indicate a tendency of tidal propagation upward throughout the year. As shown in Figures 3a–3h, the composite zonal and meridional winds during the winter solstice and spring equinox show distinct vertical structures in the diurnal tides. In Figures 3m–3p, the zonal and meridional winds during the summer solstice and autumn equinox show the composite structures of diurnal and semidiurnal tides.

To better extract and compare the tidal components observed by the two KMMRs, we process the MR wind speed data by using the method mentioned in Section 2. Figure 4 shows the monthly amplitudes and phases of the zonal and meridional diurnal tidal components. Figures 4a–4h show that the amplitudes and phases observed by the 37.5 MHz MR and the 53.1 MHz MR are essentially consistent. Typically, it can be noted that the tidal amplitude of the diurnal component in the meridional wind is relatively larger than that in the zonal wind at low latitudes, as documented previously (Yu Y et al., 2017).

Our results indicate that at low latitudes, the meridional and zonal tidal amplitudes above 86 km show the maximum during spring (February to April), reaching up to values of approximately 50 and 40 m/s, respectively. Additionally, the diurnal amplitudes exhibit a second maximum in the autumn season (September to October), following the general pattern of a strong maximum during the equinox and a weaker maximum during the solstice (Hindley et al., 2022). Note that both the 37.5 MHz MR and the 53.1 MHz MR show a short enhancement in meridional winds in July, reaching up to 40 m/s. The results indicate a high consistency in the observed amplitudes of the diurnal tide by both radars.

The zonal and meridional diurnal tidal phases observed by the two MRs at low latitudes basically remain stable throughout the year, as shown in Figures 4e–4h. All the diurnal phases indicate upwardly propagating tides. The diurnal tidal vertical wavelengths during summer and winter are generally longer than those during spring and autumn. Approximately 8- to 16-h phase lags occur between the zonal and meridional components. In general, we also find excellent agreement in the diurnal phase.

Figure 5 shows the monthly mean semidiurnal tidal amplitudes and phases observed by both the 37.5 MHz MR and the 53.1 MHz MR. In general, the distributions and variations of the semidiurnal tidal amplitudes and phases are consistent and weaker than the diurnal tides. Above 86 km, both radars show maximum zonal wind amplitudes in March to April and August to September, with the former reaching up to 20 m/s and the latter slightly lower at 16–18 m/s. Similar to the diurnal tides, the meridional semidiurnal tides are stronger than the zonal semidiurnal tides. Above 86 km, both amplitudes observed by the two radars exceed 20 m/s from January to July. Similarly, maxima are also observed in December. Figures 5e–5h show the zonal and meridional semidiurnal tidal

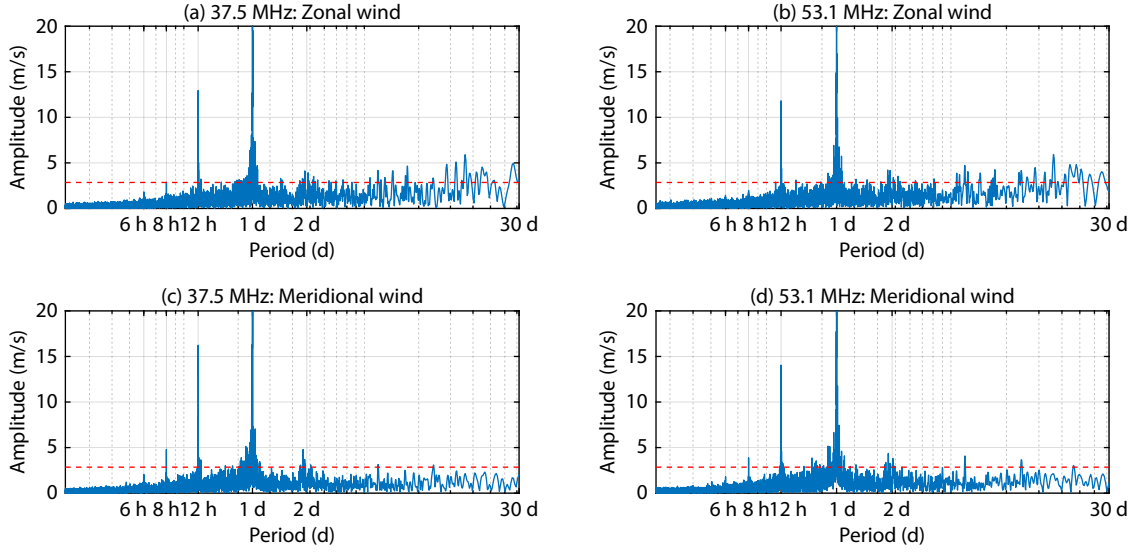

Figure 2. Lomb–Scargle periodogram of the hourly winds at 90 km altitude measured by the 37.5 MHz MR and 53.1 MHz MRs for the period from November 2013 to December 2014. The red dashed lines show the 95% confidence level.

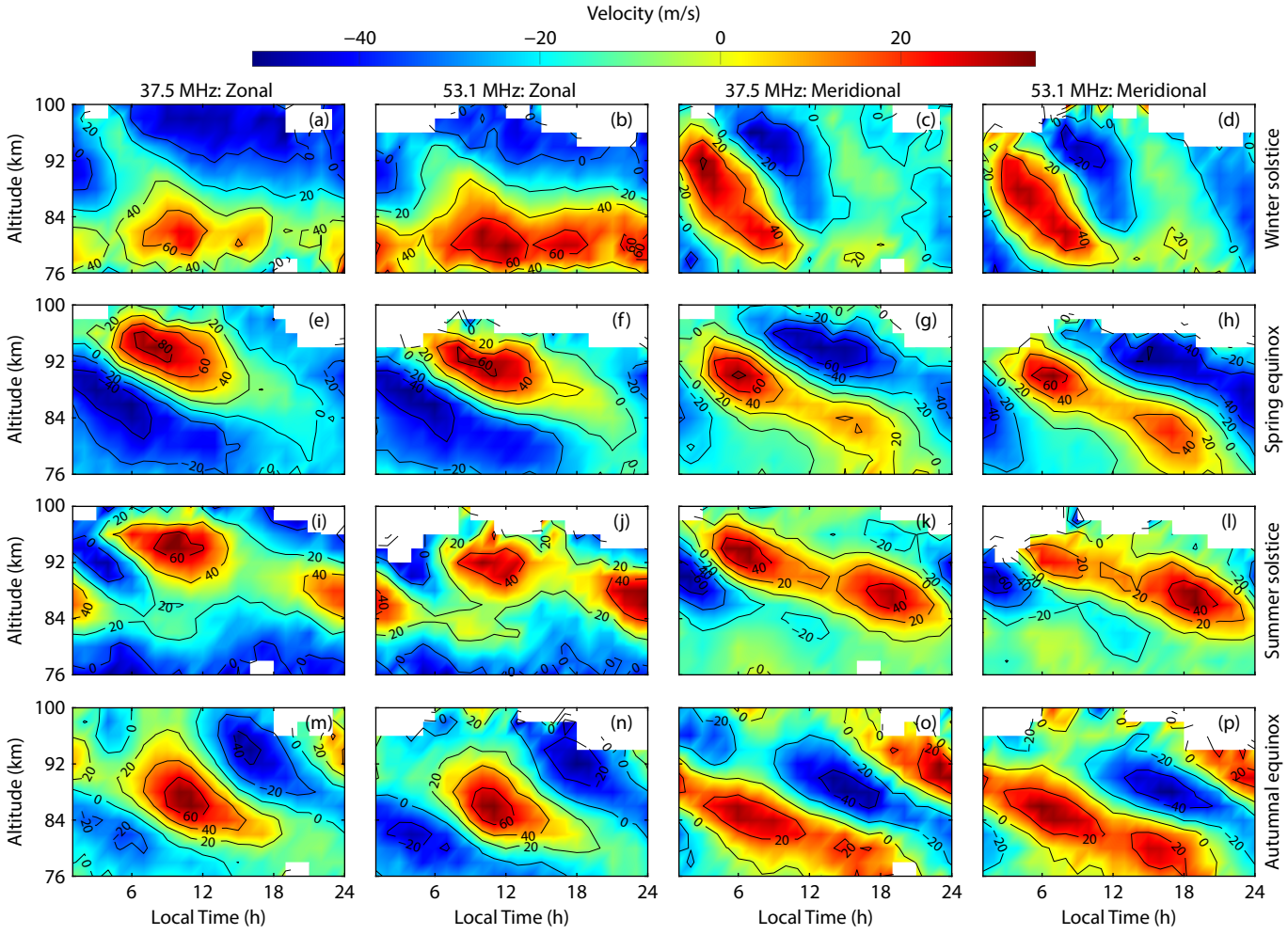

Figure 3. The 37.5 MHz MR hourly mean zonal (first column) and meridional (third column) winds and the 53.1 MHz MR hourly mean zonal (second column) and meridional (fourth column) wind composite for 21-d intervals centered on the (first row) winter solstice (2013), (second row) spring equinox, (third row) summer solstice, and (fourth row) autumn equinox over 14 months.

phases. The values of semidiurnal tidal phases generally decrease with increasing altitude, which indicates that the semidiurnal tide is again consistent with an upwardly propagating tide. Both the zonal and meridional semidiurnal tidal phases show quick phase changes during spring and autumn. An approximately 6-h (half-cycle) phase lag occurs between the zonal and meridional components.

Figure 6 shows the zonal and meridional terdiurnal tidal amplitude and phase obtained from two KMMRs. Whereas the terdiurnal tide represents the third harmonic of diurnal tidal waves and its amplitude is typically smaller, instances occur in which the terdiurnal tide can enhance and become comparable with the diurnal and semidiurnal tides (Reddi et al., 1993; Younger et al., 2002; Pancheva et al., 2013). As shown in Figure 6, similar to the diurnal and semidiurnal tides, the differences in the amplitudes and phases of the terdiurnal tides between two MR measurements are not significant. Above 90 km, both zonal and meridional winds exhibit maxima in January, March, and July, reaching up to 10 m/s. Likewise, the altitude–phase structure of the terdiurnal tides in the zonal and meridional winds observed by the two radars indicates the presence of vertically propagating waves with different vertical wavelengths. For the zonal wind, the vertical wavelengths during winter (November to February) are larger compared with those in summer (May to August). In the case of the meridional wind, terdiurnal tides exhibit smaller vertical wavelengths in winter (November to February), whereas the rest of the time, the vertical wavelengths are very large.

4. Statistical Comparison of Tides Observed by the Two Collocated Meteor Radars

For a more intuitive comparison of the tides observed by the two KMMRs, we conduct a quantitative comparison using statistical methods, similar to the approach described by Franke et al. (2005). Figure 7 shows scatterplots depicting the amplitude distributions of diurnal, semidiurnal, and terdiurnal tides observed by the two KMMRS. As shown in Figure 7, it is clear that the data from both radars exhibit exceptional similarities in all aspects of amplitude. The correlation coefficients are also large, reaching a maximum of 0.80 and mostly exceeding 0.7. Among them, the correlation coefficients of the terdiurnal tidal amplitudes between the two radars are low, falling below 0.7. This result demonstrates the consistency of the two radars in observing atmospheric tides. The

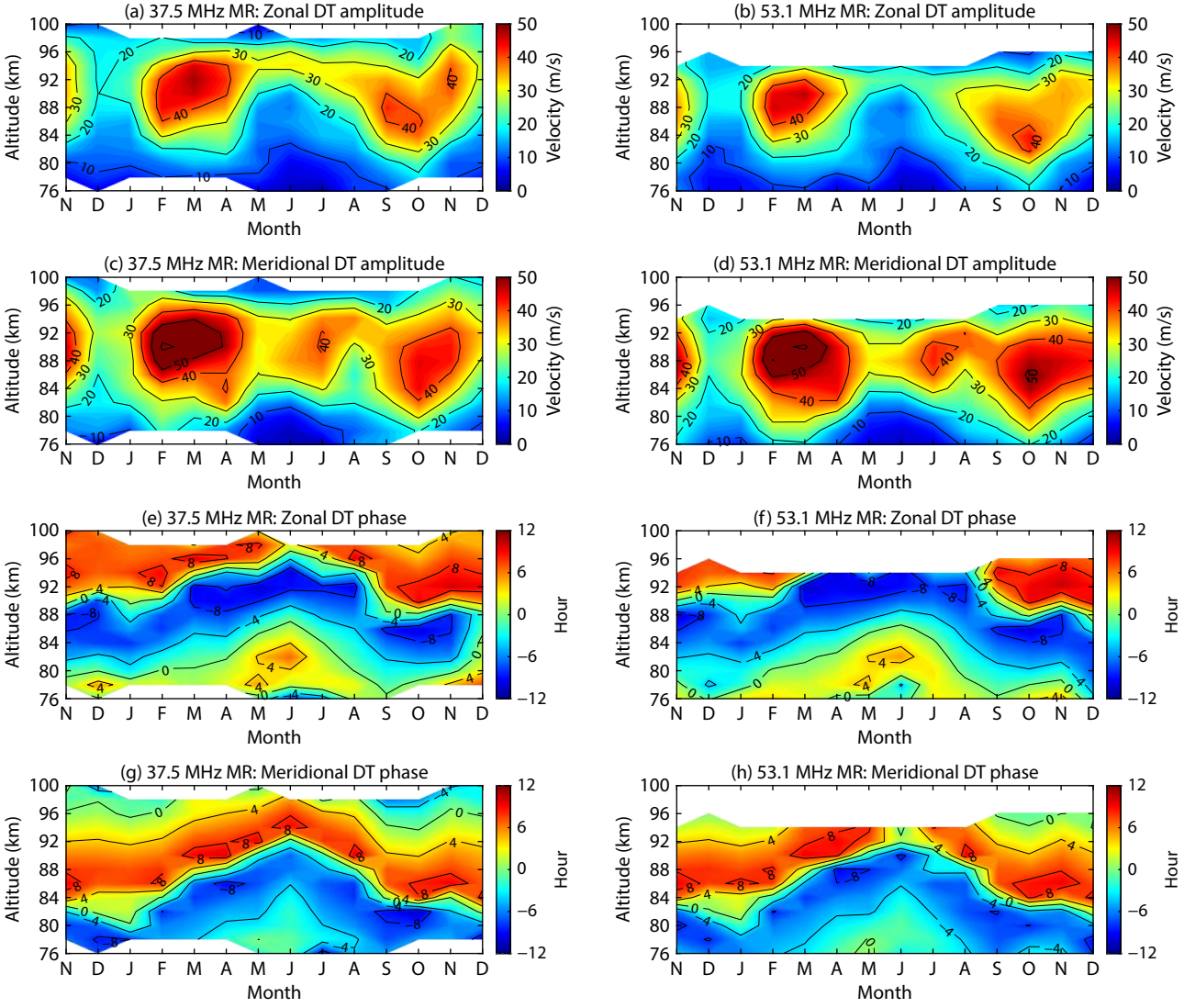

Figure 4. Composite of the zonal and meridional diurnal tidal (DT) amplitude (upper two rows) and phase (lower two rows) estimated by using the hourly wind measurements from November 2013 to December 2014 observed by the Kunming 37.5 MHz MR (left column). The right column shows the zonal and meridional DT amplitude and phase observed by the Kunming 53.1 MHz MR results.

lower correlation of the terdiurnal tidal amplitudes may be attributed to the fact that this tidal component represents the third harmonic of the wind and its smaller amplitude is an intrinsic characteristic, making it more susceptible to the influence of background noise, as evidenced in Figure 2 (Thayaparan, 1997).

Figures 8a–8f show histograms of the differences in tidal amplitudes observed by the 37.5 MHz MR and the 53.1 MHz MR. Notably, the distribution of histograms for these differences exhibits characteristics indicative of a normal distribution, as evidenced by the red smooth curves. The results also present the mean differences and confidence intervals for amplitude differences. It is noteworthy that the mean differences for amplitude are quite small, with approximate values of 0. Furthermore, their confidence intervals include 0 or are extremely close to 0. This observation indicates that no significant differences occurred between the tidal parameters observed by the 37.5 MHz MR and the 53.1 MHz MR. These results provide strong evidence that the two radar systems yield highly consistent results in the observation of tidal parameters, in terms of amplitude.

Figures 8g–8l illustrate a histogram presenting the distribution of ratios in tidal amplitudes as observed by the 37.5 MHz MR compared with the 53.1 MHz MR. This result represents the relative differences between the two MRs in terms of amplitude. The median values of these distributions are marked in the figures. A median of 1.0 indicates that in 50% of the measurements, the tidal parameters observed by the 37.5 MHz MR exceeded those observed by the 53.1 MHz MR, and vice versa.

Overall, the medians of the ratio distributions for tidal amplitudes are very close to 1.0. For the tidal amplitude ratios of the diurnal tides, the difference from 1.0 is within 3%. Similarly, for the semidiurnal tide, the difference is within 4%. However, for the terdiurnal tide, the zonal wind ratio deviates from 1.0 by approximately 5%, whereas the meridional wind ratio reaches approximately 12%. This result indicates a high degree of similarity in the diurnal and

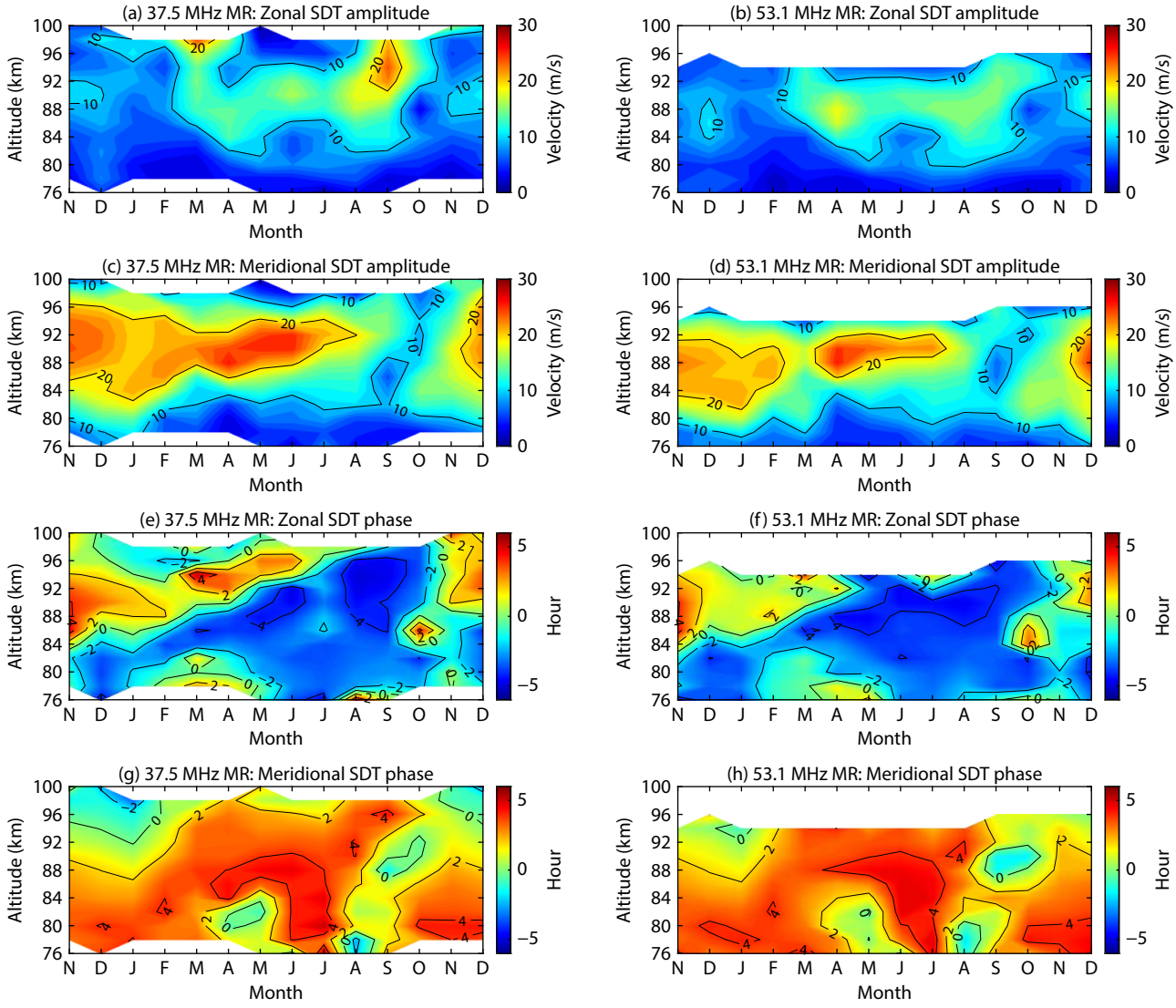

Figure 5. Same as Figure 3 but for the semidiurnal tidal (SDT) amplitude and phase components.

semidiurnal tides between the two MRs. The slightly lower comparative result for the terdiurnal tides is attributed to its increased susceptibility to interference from background noise, as mentioned above.

The preceding description provides an overall summary of the amplitude data aggregated across all altitudes. Below, we summarize the altitude dependence of amplitude. In Figures 9a–9f, we present the variance within the altitude range of 78–94 km, representing the dispersion of tidal amplitudes observed by the two MRs at all altitudes, as well as the covariance between the zonal and meridional amplitude measurements. This covariance quantifies the degree to which the zonal and meridional tidal amplitudes, observed by the 37.5 MHz MR and the 53.1 MHz MR, respectively, vary together with altitude. Please note that data at the extreme heights in the figure, far from the center, have significantly lower sample sizes, resulting in increased uncertainty. As shown in Figure 9, the variance and covariance of amplitude are quite similar, indicating a strong linear relationship among their amplitudes, with a consistent trend of variation with altitude.

Figures 9g–9i show the correlation coefficients of the amplitude between the 37.5 MHz MR and the 53.1 MHz MR. It is obvious that the correlation coefficients of the two MRs are very close to 1.0, with most of them exceeding 0.7. Notably, tidal parameters of the meridional component exhibit a higher correlation compared with the tidal parameters of the zonal component. Additionally, the figure reveals a trend in which the correlation coefficients for all amplitudes initially increase with altitude and then decrease. This result implies that data at the altitudes near both boundaries (78 and 94 km) have lower correlations, as expected, because the correlation coefficient generally rises when the meteor counts increase, and meteor counts are lower near both boundaries. This observation underscores the generally strong consistency in the tidal parameters observed by the two MRs at all altitudes.

Figure 10 illustrates the median absolute differences and root mean square (RMS) differences between the wind components of the two radars. These differences are represented by open circles and squares, respectively. The trends in median absolute differences and RMS differences in both zonal and meridional wind amplitudes are largely consistent. In terms of amplitudes, the

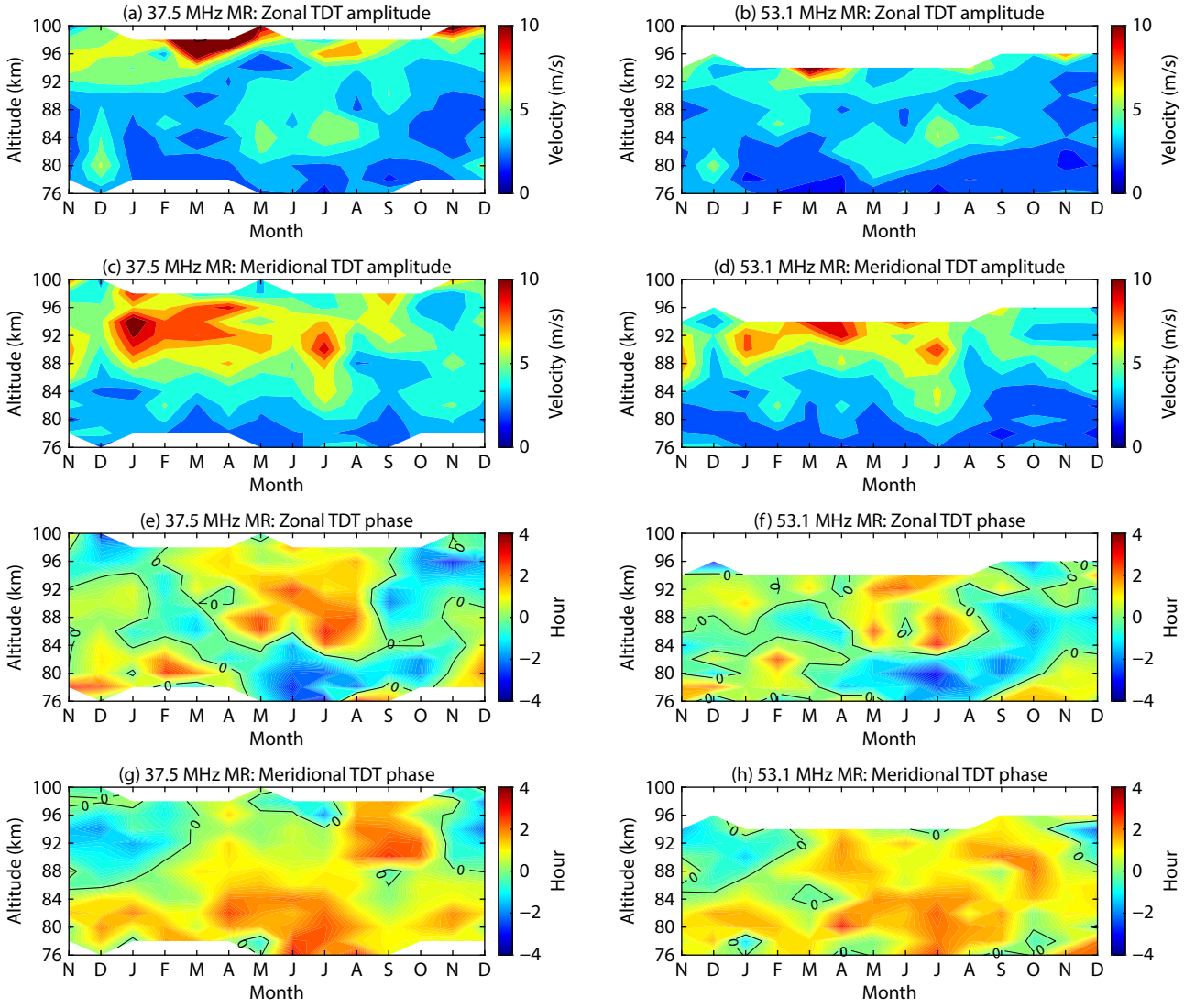

Figure 6. Same as Figure 4 but for the terdiurnal tidal (TDT) amplitude and phase components.

median absolute differences for diurnal, semidiurnal, and terdiurnal tides are in the ranges of approximately 2–4 m/s, 1–2 m/s, and 1–2 m/s, respectively. The RMS differences are within the ranges of 3–6 m/s, 2–3 m/s, and 1–2 m/s, respectively. An increase with the highest values in both the median absolute difference and the RMS difference is observed in the altitude range of 92–94 km, as expected. These values are primarily attributed to a reduction in the observed number of meteors.

To facilitate a better comparison of tidal parameters, we calculate the monthly average vertical wavelengths of the diurnal and semidiurnal tides as shown in Figure 11. The figure indicates that for both the diurnal and semidiurnal tides, the vertical wavelength trends measured by radars at both frequencies are broadly similar. Diurnal tide vertical wavelengths range between 20 and 40 km, whereas semidiurnal tide vertical wavelengths span from 25 to 75 km. For the diurnal tides, both the zonal (a) and meridional (b) vertical wavelengths exhibit relative stability throughout the year. In contrast, the semidiurnal tides demonstrate some seasonal fluctuations in both the zonal (c) and meridional (d) components, particularly during the autumn months (August to October).

Additionally, Figure 12 provides insight into the seasonal variability of the monthly mean vertical wavelength differences. It is observed that for both diurnal and semidiurnal tides, the vertical wavelength differences for the zonal and meridional components are generally consistent, remaining near the zero level throughout the different months. This consistency indicates that the vertical wavelength differences are small, with no significant bias for either diurnal or semidiurnal tides. Overall, the standard deviation of the diurnal tide vertical wavelengths is relatively stable, reflecting their consistency during the observation period. And the semidiurnal tides exhibit larger standard deviations during the summer (May and June) and winter (November), indicating increased variability in these seasons, likely related to seasonal changes in atmospheric conditions. The consistency in the tidal vertical wavelength observations from the two radars across the entire observational range lends further credibility to the reliability of the observed tidal behaviors.

5. Summary

In this study, we extract diurnal, semidiurnal, and terdiurnal tidal

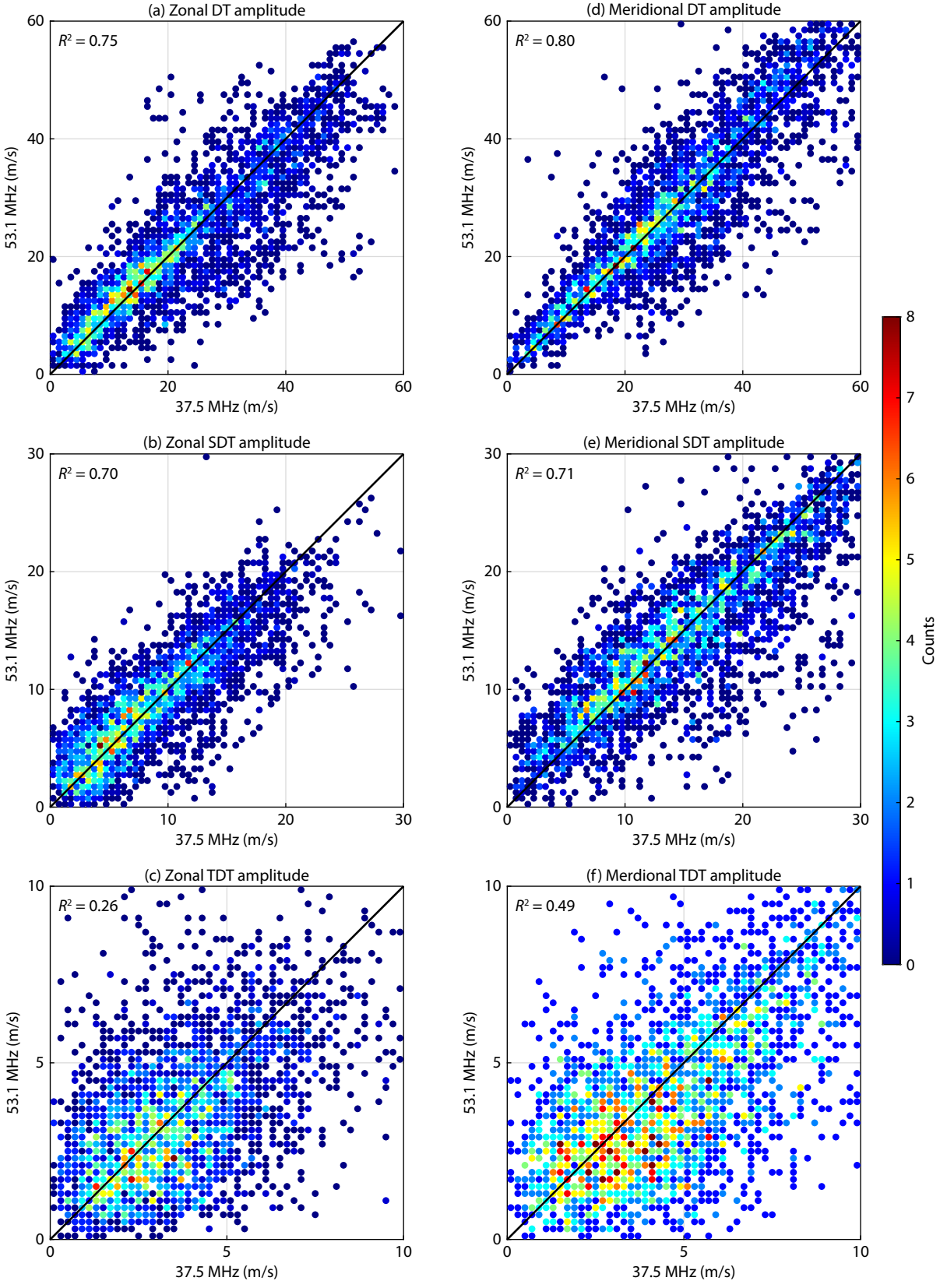

Figure 7. Scatterplots for the tidal amplitudes observed by the 37.5 MHz MR and the 53.1 MHz MR in the 76–100 km altitude range. The black line represents the diagonal.

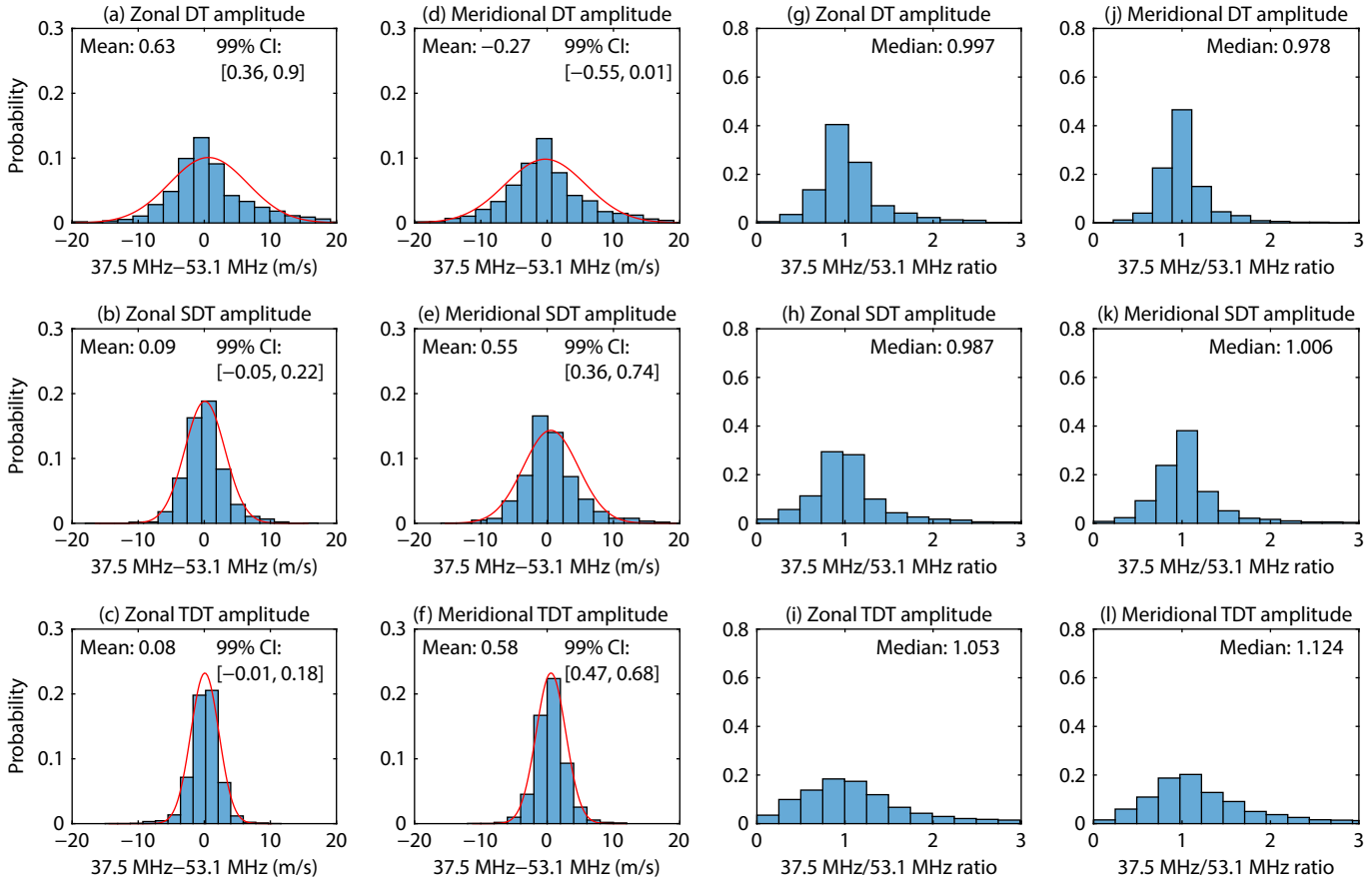

Figure 8. Combined histograms of tidal amplitude differences and ratios observed by the 37.5 MHz MR and the 53.1 MHz MR within the 76–100 km altitude range. The smooth red curves represent normal distributions, with mean and variance equal to the sample mean and variance. The mean direction differences and 99% confidence intervals are noted in panels (a) to (f). The median ratios are noted in panels (g) to (l).

components observed by the two collocated MRs of different frequencies located at low latitudes and conduct a quantitative statistical comparison of the results. The statistical findings, summarized herein, affirm the comparability of other devices with MRs in retrieving winds in the MLT region. Moreover, this work verifies reliable consistency in the performance of MRs at different operating frequencies and demonstrates the utility of MRs in observing the MLT region. The main findings can be summarized as follows:

(1) Horizontal winds in the MLT region exhibit primarily annual variations at low latitudes. Above 84 km, the zonal wind is eastward in summer and westward in winter, whereas below 84 km, it is eastward in winter and westward in spring. The meridional wind is northward during winter below 90 km and southward during spring above 90 km.

(2) The vertical tidal structures indicate an upward propagation of tides throughout the year. During the spring equinox and winter solstice, both meridional and zonal winds exhibit distinct vertical structures within the diurnal tide. In contrast, during the summer solstice and autumnal equinox, the meridional and zonal winds reveal a complex structure influenced by both diurnal and semidiurnal tides.

(3) At low latitudes, during spring, the diurnal tidal amplitude of the meridional and zonal components can reach up to 50 and 40 m/s, respectively, above 86 km. The diurnal amplitude exhibits a second maximum in autumn, closely following the strong maximum during the equinox and the weaker maximum during the winter solstice.

(4) The tidal amplitudes observed by the two collocated MRs exhibit strong consistency, with most of the correlation coefficients for the diurnal, semidiurnal, and terdiurnal tides exceeding 0.7. Throughout the entire altitude range of 78–94 km, except for the terdiurnal tide amplitudes, the correlation coefficients for the amplitudes between the two radars are relatively high, all exceeding 0.7. The 99% confidence intervals for the differences in tidal amplitudes between the 37.5 MHz MR and the 53.1 MHz MR mostly encompass zero, and the median values of the ratios are very close to 1.0. The two radars also demonstrate good consistency in the seasonal variability of tidal vertical wavelengths.

These results demonstrate the significant contributions of the two collocated low-latitude MRs to the MLT region. The comparison of both radars facilitates joint observations and validation of the atmospheric dynamics in the MLT region, providing a convenient means for studying the coupling between the lower and upper atmosphere.

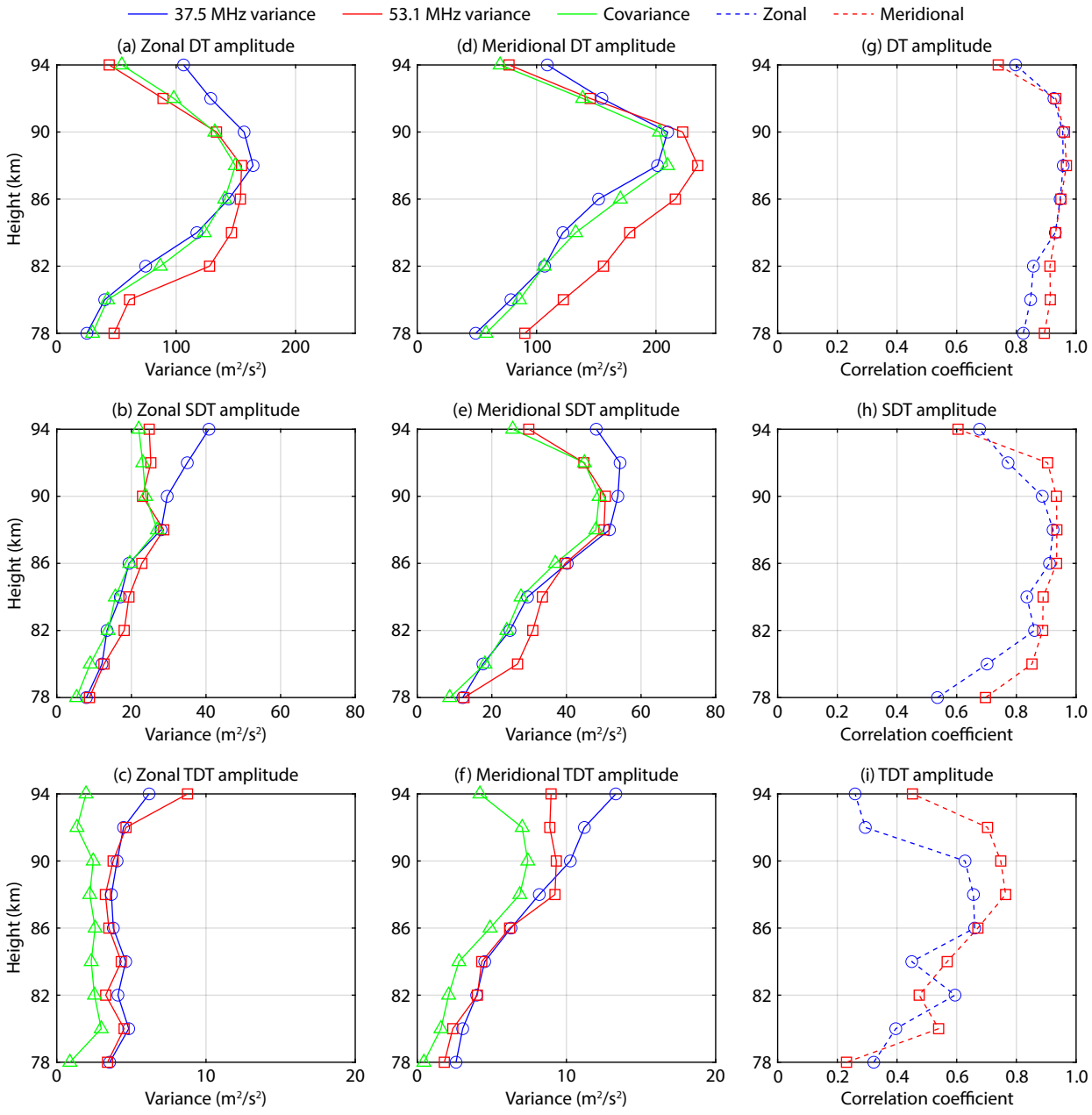

Figure 9. Variance and correlation of tidal amplitudes observed by the 37.5 MHz MR and the 53.1 MHz MR. Variance of the zonal and meridional tidal amplitudes is depicted by blue lines with circles and red lines with squares, respectively, for the 37.5 MHz MR and the 53.1 MHz MR, against altitude, with covariance shown by green lines with triangles. Correlation coefficients for meridional (blue dashed lines with circles) and zonal (red dashed lines with squares) tidal amplitudes are plotted on the right, demonstrating the relationship strength as a function of altitude.

Acknowledgments

This work was supported by the National Natural Science Foundation of China (Grant Nos. 42125402 and 42174183), the National Key Technologies R&D Program of China (Grant No. 2022YFF0503703), the B-type Strategic Priority Program of the Chinese Academy of Sciences (Grant No. XDB41000000), the foundation of the National Key Laboratory of Electromagnetic Environment and the Fundamental Research Funds for the Central Universities, and the Chinese Meridian Project. We acknowledge the data storage resources from the provision of Kunming MR data by the China Research Institute of Radiowave Propagation (CRIRP).

References

Allen, S. J., and Vincent, R. A. (1995). Gravity wave activity in the lower atmosphere: seasonal and latitudinal variations. *J. Geophys. Res.: Atmos.*, *100*(D1), 1327–1350. https://doi.org/10.1029/94JD02688

Baumgarten, K., and Stober, G. (2019). On the evaluation of the phase relation between temperature and wind tides based on ground-based measurements and reanalysis data in the middle atmosphere. *Ann. Geophys.*, *37*(4), 581–602. https://doi.org/10.5194/angeo-37-581-2019

Cervera, M. A., and Reid, I. M. (1995). Comparison of simultaneous wind measurements using colocated VHF meteor radar and MF spaced antenna radar systems. *Radio Sci.*, *30*(4), 1245–1261. https://doi.org/10.1029/95RS00644

Chapman, S., and Lindzen, R. S. (1970). *Atmospheric Tides: Thermal and Gravitational*. Dordrecht, Netherlands: Springer.

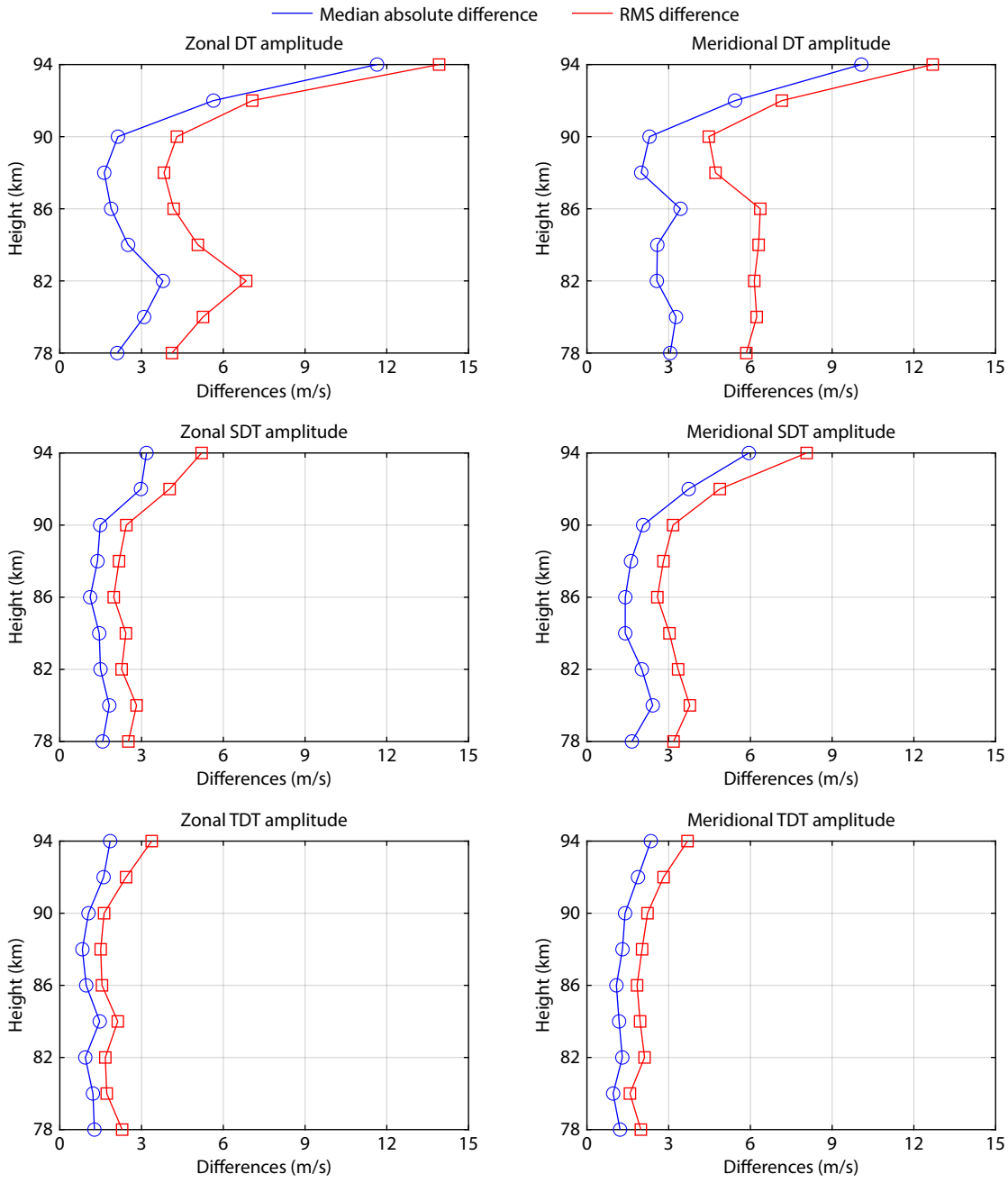

Figure 10. Median absolute difference (blue lines with circles) and RMS difference (red lines with squares) between tidal amplitudes observed by the 37.5 MHz MR and the 53.1 MHz MR versus height.

https://doi.org/10.1007/978-94-010-3399-2

Espy, P. J., Hibbins, R. E., Riggin, D. M., and Fritts, D. C. (2005). Mesospheric planetary waves over Antarctica during 2002. *Geophys. Res. Lett.*, *32*(21), L21804. https://doi.org/10.1029/2005GL023886

Forbes, J. M., and Garrett, H. B. (1979). Theoretical studies of atmospheric tides. *Rev. Geophys.*, *17*(8), 1951–1981. https://doi.org/10.1029/RG017i008p01951

Forbes, J. M. (1984). Middle atmosphere tides. *J. Atmos. Terr. Phys.*, *46*(11), 1049–1067. https://doi.org/10.1016/0021-9169(84)90008-4

Forbes, J. M. (1995). Tidal and planetary waves. In R. M. Johnson et al. (Eds.), *The Upper Mesosphere and Lower Thermosphere: A Review of Experiment and Theory* (pp. 67–87). Washington, DC: American Geophysical Union. https://doi.org/10.1029/GM087p0067

Franke, S. J., Chu, X., Liu, A. Z., and Hocking, W. K. (2005). Comparison of meteor radar and Na Doppler lidar measurements of winds in the mesopause region above Maui, Hawaii. *J. Geophys. Res.: Atmos.*, *110*(D9), D09S02. https://doi.org/10.1029/2003JD004486

Fritts, D. C., and Alexander, M. J. (2003). Gravity wave dynamics and effects in the middle atmosphere. *Rev. Geophys.*, *41*(1), 1003. https://doi.org/10.1029/2001RG000106

Gong, Y., Zhou, Q. H., and Zhang, S. D. (2013). Atmospheric tides in the low-latitude *E* and *F* regions and their responses to a sudden stratospheric warming event in January 2010. *J. Geophys. Res.: Space Phys.*, *118*(12), 7913–7927. https://doi.org/10.1002/2013ja019248

Gong, Y., Ma, Z., Li, C., Lv, X. D., Zhang, S. D., Zhou, Q. H., Huang, C. M., Huang, K. M., Yu, Y., and Li, G. Z. (2020). Characteristics of the quasi-16-day wave in the mesosphere and lower thermosphere region as revealed by meteor radar, Aura satellite, and MERRA2 reanalysis data from 2008 to 2017. *Earth Planet. Phys.*, *4*(3), 274–284. https://doi.org/10.26464/epp2020033

Gu, S. Y., Lei, J. H., Dou, X. K., Xue, X. H., Huang, F. Q., and Jia, M. J. (2017). The modulation of the quasi-two-day wave on total electron content as

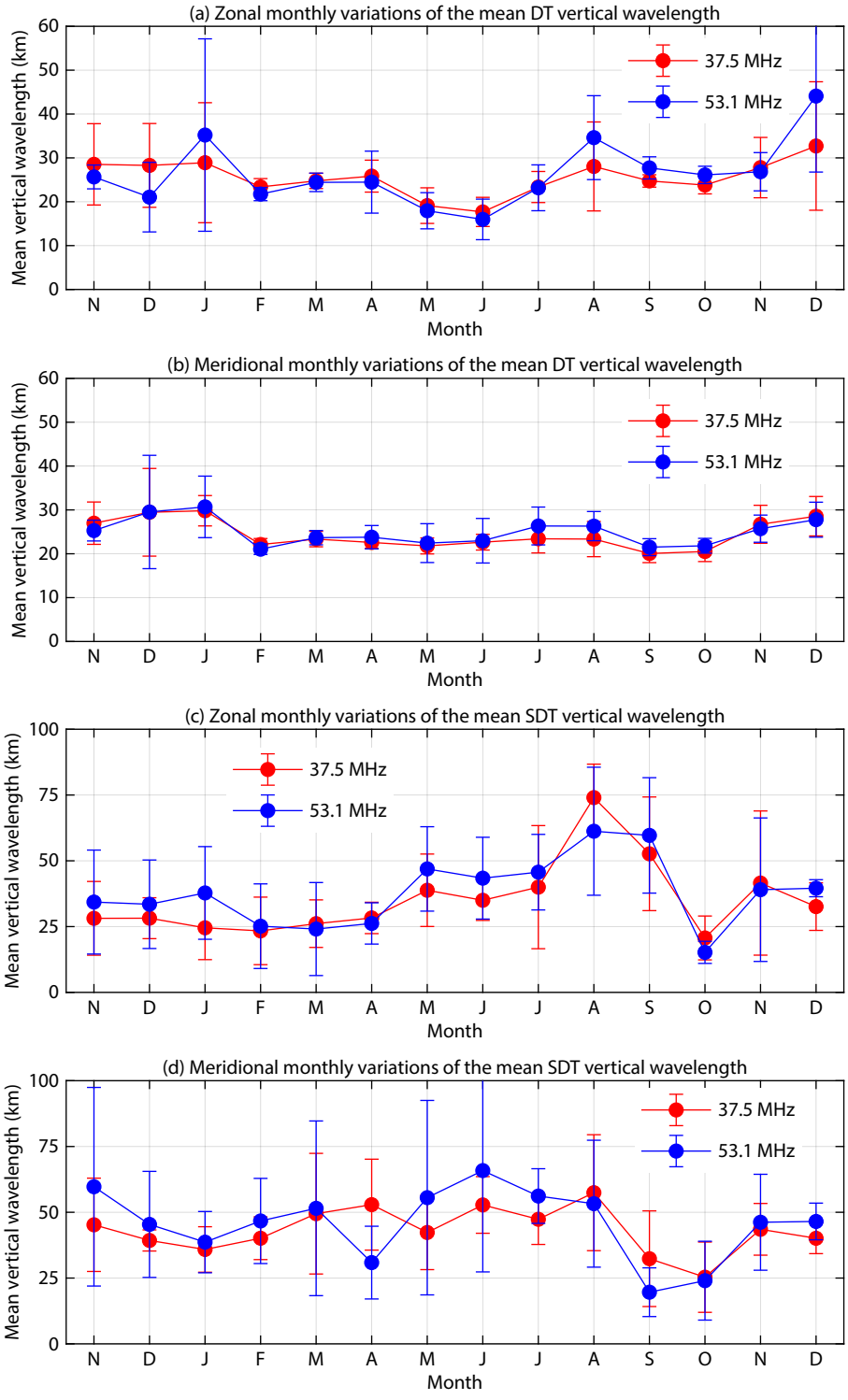

Figure 11. Monthly variations of the mean vertical wavelength from November 2013 to December 2014 observed by the two KMMRs. The red and blue lines are the monthly mean vertical wavelengths corresponding to the 37.5 MHz MR and the 53.1 MHz MR, respectively.

revealed by BeiDou GEO and meteor radar observations over central China. *J. Geophys. Res.: Space Phys.*, *122*(10), 10651–10657. https://doi.org/10.1002/2017JA024349

Gu, S. Y., Hou, X., Li, N., Yi, W., Ding, Z. H., Chen, J. S., Hu, G. Y., and Dou, X. K. (2021). First comparative analysis of the simultaneous horizontal wind observations by collocated meteor radar and FPI at low latitude through 892.0-nm airglow emission. *Remote Sens.*, *13*(21), 4337. https://doi.org/10.3390/rs13214337

Guharay, A., Batista, P. P., Clemesha, B. R., Sarkhel, S., and Buriti, R. A. (2013). On the variability of the terdiurnal tide over a Brazilian equatorial station using meteor radar observations. *J. Atmos. Sol. Terr. Phys.*, *104*, 87–95. https://doi.org/10.1016/j.jastp.2013.08.021

Hagan, M. E. (1996). Comparative effects of migrating solar sources on tidal signatures in the middle and upper atmosphere. *J. Geophys. Res.: Atmos.*, *101*(D16), 21213–21222. https://doi.org/10.1029/96JD01374

Hall, C. M., Dyrland, M. E., Tsutsumi, M., and Mulligan, F. J. (2012). Temperature

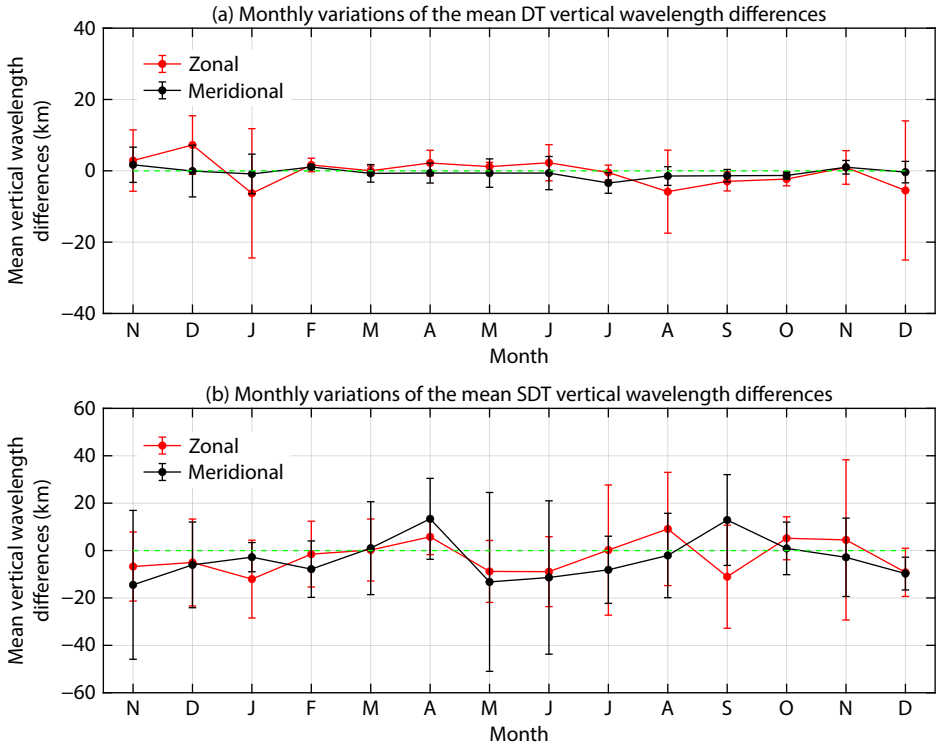

Figure 12. Monthly variations of the mean vertical wavelength differences from November 2013 to December 2014 observed by the two KMMRs. The red and black lines are the monthly mean vertical wavelength differences, with standard deviation error bars corresponding to the zonal and meridional wind components, respectively. The green dashed line represents the mean vertical wavelength difference of 0.

trends at 90 km over Svalbard, Norway (78°N 16°E), seen in one decade of meteor radar observations. *J. Geophys. Res.: Atmos.*, *117*(D8), D08104. https://doi.org/10.1029/2011JD017028

He, M. S., and Chau, J. L. (2019). Mesospheric semidiurnal tides and near-12 h waves through jointly analyzing observations of five specular meteor radars from three longitudinal sectors at boreal midlatitudes. *Atmos. Chem. Phys.*, *19*(9), 5993–6006. https://doi.org/10.5194/acp-19-5993-2019

He, M. S., and Forbes, J. M. (2022). Rossby wave second harmonic generation observed in the middle atmosphere. *Nat. Commun.*, *13*(1), 7544. https://doi.org/10.1038/s41467-022-35142-3

He, M. S. (2023). Planetary-scale MLT waves diagnosed through multi-station methods: a review. *Earth, Planets Space*, *75*(1), 63. https://doi.org/10.1186/s40623-023-01808-5

Hindley, N. P., Mitchell, N. J., Cobbett, N., Smith, A. K., Fritts, D. C., Janches, D., Wright, C. J., and Moffat-Griffin, T. (2022). Radar observations of winds, waves and tides in the mesosphere and lower thermosphere over South Georgia island (54° S, 36° W) and comparison with WACCM simulations. *Atmos. Chem. Phys.*, *22*(14), 9435–9459. https://doi.org/10.5194/acp-22-9435-2022

Hocking, W. K., and Thayaparan, T. (1997). Simultaneous and colocated observation of winds and tides by MF and meteor radars over London, Canada (43°N, 81°W), during 1994–1996. *Radio Sci.*, *32*(2), 833–865. https://doi.org/10.1029/96RS03467

Hocking, W. K. (1999). Temperatures Using radar-meteor decay times. *Geophys. Res. Lett.*, *26*(21), 3297–3300. https://doi.org/10.1029/1999GL003618

Hocking, W. K., Thayaparan, T., and Franke, S. J. (2001). Method for statistical comparison of geophysical data by multiple instruments which have differing accuracies. *Adv. Space Res.*, *27*(6-7), 1089–1098. https://doi.org/10.1016/S0273-1177(01)00143-0

Holdsworth, D. A., Reid, I. M., and Cervera, M. A. (2004). Buckland Park all-sky interferometric meteor radar. *Radio Sci.*, *39*(5), RS5009. https://doi.org/10.1029/2003RS003014

Jacobi, C., Krug, A., and Merzlyakov, E. (2017). Radar observations of the quarterdiurnal tide at midlatitudes: seasonal and long-term variations. *J. Atmos. Sol. Terr. Phys.*, *163*, 70–77. https://doi.org/10.1016/j.jastp.2017.05.014

Kishore, P., Velicogna, I., Sutterley, T. C., Mohajerani, Y., Ciracì, E., and Madhavi, G. N. (2018). A case study of mesospheric planetary waves observed over a three-radar network using empirical mode decomposition. *Ann. Geophys.*, *36*(3), 925–936. https://doi.org/10.5194/angeo-36-925-2018

Liu, G. P., Janches, D., Ma, J., Lieberman, R. S., Stober, G., Moffat-Griffin, T., Mitchell, N. J., Kim, J. H., Lee, C., and Murphy, D. J. (2022). Mesosphere and lower thermosphere winds and tidal variations during the 2019 antarctic sudden stratospheric warming. *J. Geophys. Res.: Space Phys.*, *127*(3), e2021JA030177. https://doi.org/10.1029/2021JA030177

Lomb, N. R. (1976). Least-squares frequency analysis of unequally spaced data. *Astrophys. Space Sci.*, *39*(2), 447–462. https://doi.org/10.1007/bf00648343

Long, C., Yu, T., Sun, Y. Y., Yan, X. X., Zhang, J., Yang, N., Wang, J., Xia, C. L., Liang, Y., and Ye, H. L. (2023). Atmospheric gravity wave derived from the neutral wind with 5-minute resolution routinely retrieved by the meteor radar at mohe. *Remote Sens.*, *15*(2), 296. https://doi.org/10.3390/rs15020296

Pancheva, D., Mukhtarov, P., and Smith, A. K. (2013). Climatology of the migrating terdiurnal tide (TW3) in SABER/TIMED temperatures. *J. Geophys. Res.: Space Phys.*, *118*(4), 1755–1767. https://doi.org/10.1002/jgra.50207

Pancheva, D., Mukhtarov, P., Hall, C., Smith, A. K., and Tsutsumi, M. (2021). Climatology of the short-period (8-h and 6-h) tides observed by meteor radars at Tromsø and Svalbard. *J. Atmos. Sol. Terr. Phys.*, *212*, 105513. https://doi.org/10.1016/j.jastp.2020.105513

Reddi, C. R., Rajeev, K., and Geetha, R. (1993). Tidal winds in the radio-meteor region over Trivandrum (8.5°N, 77°E). *J. Atmos. Terr. Phys.*, *55*(9), 1219–1231. https://doi.org/10.1016/0021-9169(93)90049-5

Reid, I. M., Holdsworth, D. A., Morris, R. J., Murphy, D. J., and Vincent, R. A. (2006). Meteor observations using the Davis mesosphere-stratosphere-troposphere radar. *J. Geophys. Res.: Space Phys.*, *111*(A5), A05305. https://doi.org/10.1029/2005JA011443

Scargle, J. D. (1982). Studies in astronomical time series analysis. II. Statistical aspects of spectral analysis of unevenly spaced data. *Astrophysical Journal*, *263*, 835–853. https://doi.org/10.1086/160554

Spargo, A. J., Reid, I. M., and MacKinnon, A. D. (2019). Multistatic meteor radar observations of gravity-wave–tidal interaction over southern Australia. *Atmos. Meas. Tech.*, *12*(9), 4791–4812. https://doi.org/10.5194/amt-12-4791-2019

Stober, G., Matthias, V., Brown, P., and Chau, J. L. (2014). Neutral density variation from specular meteor echo observations spanning one solar cycle. *Geophys. Res. Lett.*, *41*(19), 6919–6925. https://doi.org/10.1002/2014GL061273

Stober, G., Kuchar, A., Pokhotelov, D., Liu, H. X., Liu, H. L., Schmidt, H., Jacobi, C., Baumgarten, K., Brown, P., … Mitchell, N. (2021). Interhemispheric differences of mesosphere–lower thermosphere winds and tides investigated from three whole-atmosphere models and meteor radar observations. *Atmos. Chem. Phys.*, *21*(18), 13855–13902. https://doi.org/10.5194/acp-21-13855-2021

Takahashi, H., Nakamura, T., Tsuda, T., Buriti, R. A., and Gobbi, D. (2002). First measurement of atmospheric density and pressure by meteor diffusion coefficient and airglow OH temperature in the mesopause region. *Geophys. Res. Lett.*, *29*(8), 1165. https://doi.org/10.1029/2001GL014101

Thayaparan, T. (1997). The terdiurnal tide in the mesosphere and lower thermosphere over London, Canada (43°N, 81°W). *J. Geophys. Res.: Atmos.*, *102*(D18), 21695–21708. https://doi.org/10.1029/97JD01839

Vial, F. (1989). Tides in the middle atmosphere. *J. Atmos. Terr. Phys.*, *51*(1), 3–17. https://doi.org/10.1016/0021-9169(89)90069-X

Vincent, R. A. (2015). The dynamics of the mesosphere and lower thermosphere: a brief review. *Prog. Earth Planet. Sci.*, *2*(1), 4. https://doi.org/10.1186/s40645-015-0035-8

Vitharana, A., Du, J., Zhu, X. W., Oberheide, J., and Ward, W. E. (2021). Numerical prediction of the migrating diurnal tide total variability in the mesosphere and lower thermosphere. *J. Geophys. Res.: Space Phys.*, *126*(11), e2021JA029588. https://doi.org/10.1029/2021ja029588

Wang, J. C., Palo, S. E., Forbes, J. M., Marino, J., Moffat-Griffin, T., and Mitchell, N. J. (2021). Unusual quasi 10-day planetary wave activity and the ionospheric response during the 2019 Southern Hemisphere sudden stratospheric warming. *J. Geophys. Res.: Space Phys.*, *126*(6), e2021JA029286. https://doi.org/10.1029/2021JA029286

Wang, J. Y., Yi, W., Wu, J. F., Chen, T. D., Xue, X. H., Zeng, J., Vincent, R. A., Reid, I. M., Batista, P. P., … Dou, X. K. (2022). Coordinated observations of migrating tides by multiple meteor radars in the equatorial mesosphere and lower thermosphere. *J. Geophys. Res.: Space Phys.*, *127*(12), e2022JA030678. https://doi.org/10.1029/2022JA030678

Wu, D. L., Hays, P. B., and Skinner, W. R. (1995). A least squares method for spectral analysis of space-time series. *J. Atmos. Sci.*, *52*(20), 3501–3511. https://doi.org/10.1175/1520-0469(1995)052<3501:ALSMFS>2.0.CO;2

Xiong, C., Zhou, Y. L., Lühr, H., and Ma, S. Y. (2015). Tidal signatures of the thermospheric mass density and zonal wind at midlatitude: CHAMP and GRACE observations. *Ann. Geophys.*, *33*(2), 185–196. https://doi.org/10.5194/angeo-33-185-2015

Yi, W., Chen, J. S., Ma, C. B., Li, N., and Zhao, Z. W. (2014). Observation of upper atmospheric temperature by Kunming all-sky meteor radar. *Chin. J. Geophys.*, *57*(5), 750–760. https://doi.org/10.1002/cjg2.20138

Yi, W., Xue, X. H., Reid, I. M., Younger, J. P., Chen, J. S., Chen, T. D., and Li, N. (2018). Estimation of mesospheric densities at low latitudes using the Kunming meteor radar together with SABER temperatures. *J. Geophys. Res.: Space Phys.*, *123*(4), 3183–3195. https://doi.org/10.1002/2017JA025059

Yi, W., Xue, X. H., Chen, J. S., Chen, T. D., and Li, N. (2019). Quasi-90-day oscillation observed in the MLT region at low latitudes from the Kunming meteor radar and SABER. *Earth Planet. Phys.*, *3*(2), 136–146. https://doi.org/10.26464/epp2019013

Yi, W., Xue, X. H., Zeng, J., Wang, J. Y., Zhou, B. Z., Ye, H. L., Chen, T. D., and Dou, X. K. (2023). Observation of MLT region winds and tides by the USTC Mengcheng meteor radar. *JUSTC*, *53*(5), 0501. https://doi.org/10.52396/JUSTC-2022-0158

Younger, P. T., Pancheva, D., Middleton, H. R., and Mitchell, N. J. (2002). The 8-hour tide in the Arctic mesosphere and lower thermosphere. *J. Geophys. Res.: Space Phys.*, *107*(A12), 1420. https://doi.org/10.1029/2001ja005086

Yu, Y., Wan, W. X., Ning, B. Q., Liu, L. B., Wang, Z. G., Hu, L. H., and Ren, Z. P. (2013). Tidal wind mapping from observations of a meteor radar chain in December 2011. *J. Geophys. Res.: Space Phys.*, *118*(5), 2321–2332. https://doi.org/10.1029/2012JA017976

Yu, Y., Wan, W. X., Reid, I. M., Chen, J. S., Vincent, R. A., Ning, B. Q., Murphy, D. J., Yang, G. T., Xue, X. H., … Zhang, Y. (2017). Global tidal mapping from observations of a radar campaign. *Adv. Space Res.*, *60*(1), 130–143. https://doi.org/10.1016/j.asr.2017.03.037

Zeng, J., Yi, W., Xue, X. H., Reid, I., Hao, X. J., Li, N., Chen, J. S., Chen, T. D., and Dou, X. K. (2022). Comparison between the mesospheric winds observed by two collocated meteor radars at low latitudes. *Remote Sens.*, *14*(10), 2354. https://doi.org/10.3390/rs14102354

Zhou, B. Z., Xue, X. H., Yi, W., Ye, H. L., Zeng, J., Chen, J. S., Wu, J. F., Chen, T. D., and Dou, X. K. (2022). A comparison of MLT wind between meteor radar chain data and SD-WACCM results. *Earth Planet. Phys.*, *6*(5), 451–464. https://doi.org/10.26464/epp2022040